



UNIVERSIDADE ESTADUAL DE CAMPINAS  
SISTEMA DE BIBLIOTECAS DA UNICAMP  
REPOSITÓRIO DA PRODUÇÃO CIENTÍFICA E INTELLECTUAL DA UNICAMP

**Versão do arquivo anexado / Version of attached file:**

Versão do Editor / Published Version

**Mais informações no site da editora / Further information on publisher's website:**

<https://journals.sagepub.com/doi/10.1177/1077546320924253>

**DOI: 10.1177/1077546320924253**

**Direitos autorais / Publisher's copyright statement:**

©2021 by Sage. All rights reserved.

DIRETORIA DE TRATAMENTO DA INFORMAÇÃO

Cidade Universitária Zeferino Vaz Barão Geraldo

CEP 13083-970 – Campinas SP

Fone: (19) 3521-6493

<http://www.repositorio.unicamp.br>

# Direct inverse control for active vibration suppression using artificial neural networks

William Camilo Ariza-Zambrano  and Alberto Luiz Serpa

Journal of Vibration and Control  
2021, Vol. 27(1–2) 31–42  
© The Author(s) 2020  
Article reuse guidelines:  
[sagepub.com/journals-permissions](https://sagepub.com/journals-permissions)  
DOI: 10.1177/1077546320924253  
[journals.sagepub.com/home/jvc](https://journals.sagepub.com/home/jvc)  


## Abstract

In this article, a control method based on artificial neural networks applied to the vibration control of flexible structures is presented. The direct inverse control method is used. This method consists in the identification of the inverse dynamics of the plant using an artificial neural network to be used as the controller. An application example is proposed, and two problem variations are treated. The application problem is based on a cantilever plate model. The plate model is obtained using the finite element method. For the first problem, the controller is designed using the full-order plant model. In the second example, a model reduction is made to evaluate the performance of this technique applied to control problems with dynamic uncertainties. The results were evaluated according to the time response and frequency response of the closed-loop system. To compare the results obtained using the control method based on artificial neural networks, the previous examples were also solved using the  $\mathcal{H}_\infty$  control method. The obtained results show that the control method based on the inverse model using neural networks is effective in solving this kind of problem.

## Keywords

Vibration control, artificial neural networks, inverse dynamic, finite element method, dynamic uncertainties

## 1. Introduction

Mechanical systems with mass, stiffness, and damping present a vibratory response when exposed to time-varying disturbances. The prediction and control of the behavior of those systems in the presence of these disturbances are important to the design and operation of mechanical equipment and structures (Fuller et al., 1996). The active vibration control uses the superposition of waves by generating a secondary signal to attenuate the undesired source, resulting in a reduction in the level of vibration in the desired location. In general, active vibration control is more effective than passive methods of vibration suppression (Darus and Tokhi, 2005).

In the literature, different approaches to vibration control in flexible structures are found. Some of the most used techniques are optimal linear quadratic Gaussian control (Banavar and Dominic, 1995; Lim et al., 1992),  $\mathcal{H}_2$  control (Lublin and Athans, 1994), and robust controllers  $\mathcal{H}_\infty$  (Moser, 1993; Smith et al., 1994; Sznaier and Rotstein, 1992). A growing group of techniques used in the solution to this kind of problem is in the *artificial intelligence* area. Methods such as fuzzy logic controllers (Forrai et al., 2000), genetic algorithms (Kundu et al., 2002), and mostly artificial neural networks have been used. Works that use artificial neural networks in cooperation with, or as a part of, more classical techniques can be found (Bittanti and Piroddi,

1993; Chun-Lian and Tsai-Yuan, 2002; Fuli et al., 1997; Faouzi et al., 2004). In some approaches, it is possible to find applications where artificial neural networks are used as a unique control mechanism (Abreu et al., 2000; Gates et al., 1993; Tavakolpour et al., 2010).

In this study, the problem of vibration control of flexible structures is treated. The control system is based on the identification of the inverse dynamics of the plant to be used as a controller. Theoretically, if the inverse plant model can be identified, this becomes the optimal controller. This technique is generally referred to as the direct inverse control method (Nørgaard et al., 2004).

In this work, the inverse plant model is identified by an artificial neural network. The ability of artificial neural networks to model a wide range of types of systems in different applications can reduce the time spent on the development of control systems, and in some cases, it offers

---

Department of Computational Mechanics, School of Mechanical Engineering, University of Campinas — UNICAMP, Brazil

Received: 24 August 2019; accepted: 12 April 2020

### Corresponding author:

Alberto Luiz Serpa, School of Mechanical Engineering, Universidade Estadual de Campinas, Rua Mendeleev 200, Cidade Universitária Zeferino Vaz, Campinas 13083–860, SP, Brazil.  
Email: [serpa@fem.unicamp.br](mailto:serpa@fem.unicamp.br)

better performance than some control techniques. This technique can be considered simple when concerning formulation and generalization, and it can be applied to numerous control problems. For example this technique is useful in problems where the plant model is unknown, or its deduction is considered difficult. Problems with nonlinearities can also be approached.

The vibration problem in a cantilever plate is studied in this work. Two application problem cases are treated. In the first case, the plant is represented by a full-order finite element model of a plate. Moreover, in the second case, a reduction of the plant model is made to evaluate the control system performance under dynamic uncertainties. The controller design using a reduced model characterizes a nonconvex optimization problem (Canahuire and Serpa, 2017). This approach can be considered more realistic because the reduced model does not have all the dynamic effects of the real plant.

This work begins by presenting the direct inverse control scheme based on artificial neural networks. The formulation of the application problems, results, and discussion are presented. Finally, conclusions and references cited in the text are listed.

## 2. Direct inverse method

The objective of this method is to identify the inverse model of the plant and use it as a controller. A summary of this method is presented as follows. The plant model is described by the discrete transfer function  $G(z)$

$$G(z) = \frac{Y(z)}{U(z)} \quad (1)$$

with  $Y(z)$  and  $U(z)$  being the output of the plant and the applied control effort, respectively. Transfer functions are defined in terms of  $z$ , which is the corresponding variable of the  $\mathbb{Z}$ -transform domain.

Furthermore, letting the controller model  $K(z)$  be the approximated inverse model of the plant  $\hat{G}^{-1}(z)$

$$K(z) = \hat{G}^{-1}(z) = \frac{\hat{U}(z)}{Y(z)} \quad (2)$$

where  $\hat{U}(z)$  is the estimated control effort for a specific plant output  $Y(z)$ . Replacing the controller's input  $Y(z)$  by the desired reference  $R(z)$ , the output of the controller is

$$\hat{U}(z) = R(z)K(z) \quad (3)$$

Letting the control effort  $U(z)$  of the plant be computed by  $K(z)$ , the output of the plant  $Y(z)$  is

$$Y(z) = U(z)G(z) = R(z)K(z)G(z) \quad (4)$$

or

$$Y(z) = R(z) \frac{\hat{U}(z)}{Y(z)} \frac{Y(z)}{U(z)} = R(z) \frac{\hat{U}(z)}{U(z)} \quad (5)$$

An exact inverse model implies  $U(z) = \hat{U}(z)$ . So, if  $K(z)$  represents the exact inverse model of  $G(z)$ ,  $K(z)$  would be the ideal controller, that is  $Y(z) = R(z)$ . This control diagram is seen in Figure 1.

An artificial neural network (ANN) can be used as a controller  $K(z)$ . ANNs are mathematical regressor models that, in the generic sense, can learn a nonlinear mapping from a set of observations (Nørgaard et al., 2004). So, an ANN can be used to identify the inverse model of the plant. That is let  $f(\theta, y_i)$  be the ANN model function in terms of the network parameters  $\theta$  and the measured plant output  $y$  at instant  $i$ . The optimal parameters  $\theta^*$  can be obtained as

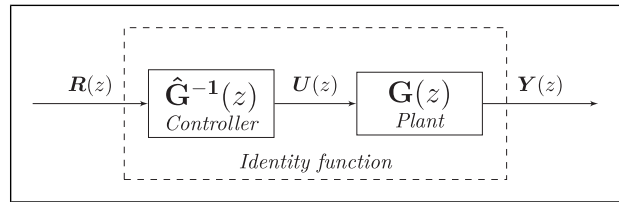


Figure 1. Direct inverse control method—conceptual idea.

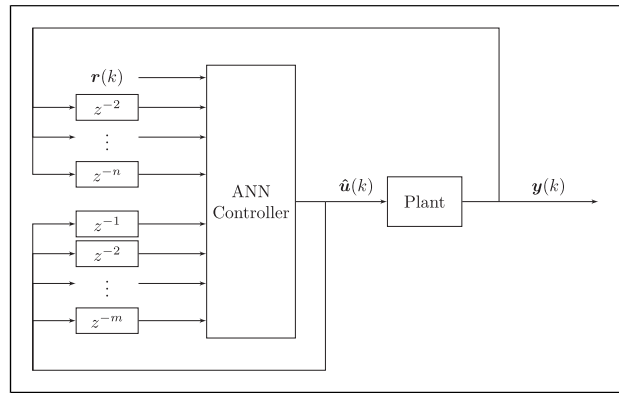


Figure 2. Direct inverse closed-loop system.

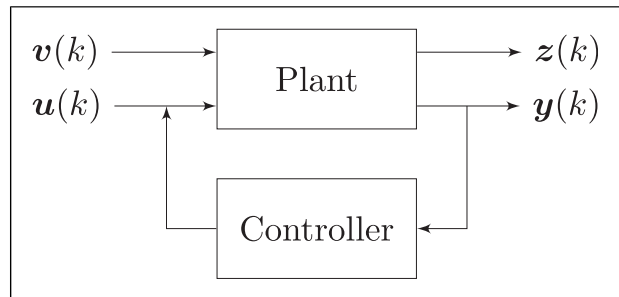


Figure 3. Closed-loop control system.

$$\theta^* = \arg \min_{\theta} \frac{1}{N} \sum_{i=1}^N [\mathbf{u}_i - \mathbf{f}(\theta, \mathbf{y}_i)]^2 \quad (6)$$

where  $\mathbf{u}_i$  is the excitation signal applied to the plant at instant  $i$  from a set of  $N$  collected data pairs  $\{\mathbf{u}_i, \mathbf{y}_i\}$ . It is worth saying that the collected observations can be obtained by a computational model simulation or by direct measurements in an experiment.

It is common to include, as the input of the controller, a set of delays of both the plant's input and output. These

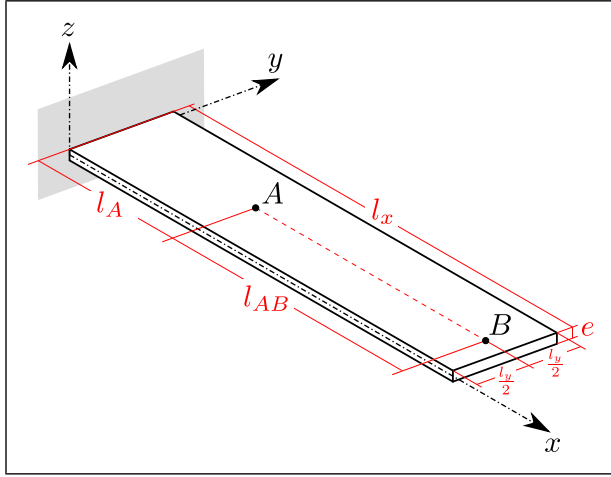


Figure 4. Clamped plate scheme.

delay inclusions are made to provide information about past states of the system to the controller. Therefore, a more accurate representation of the inverse dynamics is expected. Thus, the controller can have as input the last  $n$  values of the plant output and the past  $m$  control signal values, that is  $\mathbf{f}(\theta, \mathbf{y}_i)$  turns in

$$\mathbf{f}(\theta, \mathbf{y}_i, \mathbf{y}_{i-1}, \dots, \mathbf{y}_{i-n}, \mathbf{u}_{i-1}, \dots, \mathbf{u}_{i-m}) \quad (7)$$

once the controller parameters have been obtained by equation (6) and to close the control loop. It is required to set the most recent output of the plant  $\mathbf{y}(k - 1)$  to the desired reference signal  $\mathbf{r}(k)$ . The closed control loop is illustrated in Figure 2. In this figure, the operator  $z^{-n}$  in the  $\mathbb{Z}$ -transform domain holds and delays its input by  $n$  sampling periods.

This control scheme has the following advantages: it is intuitively simple, easy to implement, and the controller can be optimized for a specific reference trajectory. On the other hand, as disadvantages, the controller design lacks the adjustment of parameters related to time response or overshoot percentage, and in general, it has a high sensitivity to disturbance and noise (Nørgaard et al., 2004).

### 3. Active vibration control applications

In the active vibration control area, the objective is to reduce the effect of disturbance  $\mathbf{v}(k)$  on performance output  $\mathbf{z}(k)$ . The controller receives as input the measured plant output  $\mathbf{y}(k)$  and generates the control signal  $\mathbf{u}(k)$ . This scheme is shown in Figure 3.

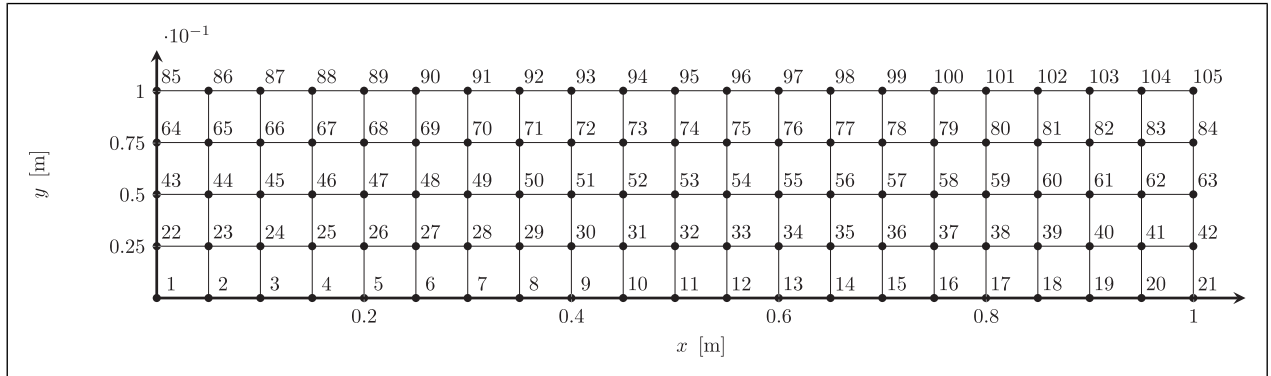
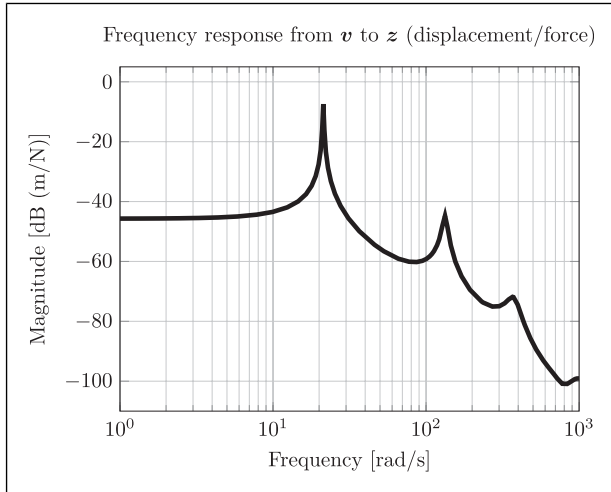


Figure 5. Cantilever plate finite element mesh.

Table I. Damping ratio and natural frequencies.

Mode	Pole	Damping ratio (%)	Natural frequency (rad/s)
1	$-0.138 \pm 21.300i$	0.64988	21,300
2	$-2.998 \pm 109.016i$	2.74937	109,058
3	$-4.456 \pm 133.062i$	3.34721	133,137
4	$-30.461 \pm 347.591i$	8.73025	348,923
5	$-35.369 \pm 374.332i$	9.40665	376,000

In this section, a vibration control problem in a cantilever plate is presented. The cantilever plate model is obtained by the finite element method (FEM) using the formulation of a rectangular plate in bending given in Przemieniecki (1985). The plant model is based on the structural dynamic equation, and it uses the proportional damping concept as defined in Rayleigh (1877). Two problem



**Figure 6.** Frequency response of the cantilever plate model from  $\mathbf{v}$  to  $\mathbf{z}$ . The three peaks correspond to vibration modes 1, 3, and 5. Modes 2 and 4 are torsional modes (Figure 7) and they remain not evident in this diagram.

variations were tested. In the first case, the controller was designed using the full-order plant model. Also, in the second case, for the controller design, a model reduction of the plant was made. A more complete description of the plant model is presented in Appendix 1.

### 3.1. Cantilever plate

Consider an aluminum plate clamped at one of its tips, as shown in Figure 4, with  $l_x = 1$  m,  $l_y = 0.05$  m,  $e = 0.01$  m,  $l_A = 0.35$  m, and  $l_{AB} = 0.6$  m. The disturbance  $\mathbf{v}$  is a concentrated force in the direction of the axis  $z$  applied in  $A$ . The control effort  $\mathbf{u}$  is a concentrated force in the direction of the axis  $z$  applied in  $B$ . Both, the output performance  $\mathbf{z}$  and control measurement  $\mathbf{y}$  are the displacement in  $z$  direction of point  $B$ . This is a collocated control problem because the location of the sensor coincides with the location of the actuator.

The plant model was obtained by using the FEM. The plate was discretized in 80 rectangular plate elements. The number of elements arranged horizontally along the axis  $x$  is 20, and the number of elements vertically disposed on the axis  $y$  is 4. The finite element mesh used is shown in Figure 5.

The mass matrix  $\mathcal{M}$  and the stiffness matrix  $\mathcal{K}$  were obtained using the finite element formulation described in Przemieniecki (1985). This formulation considers a rectangular element with four nodes placed in the element vertices. Each node has 3 degrees of freedom, a displacement in  $z$  axis direction, and rotations in  $x$  and  $y$  axes. The damping matrix  $\mathcal{C}$  was obtained by  $\mathcal{C} = \alpha_1 \mathcal{K} + \alpha_2 \mathcal{M}$

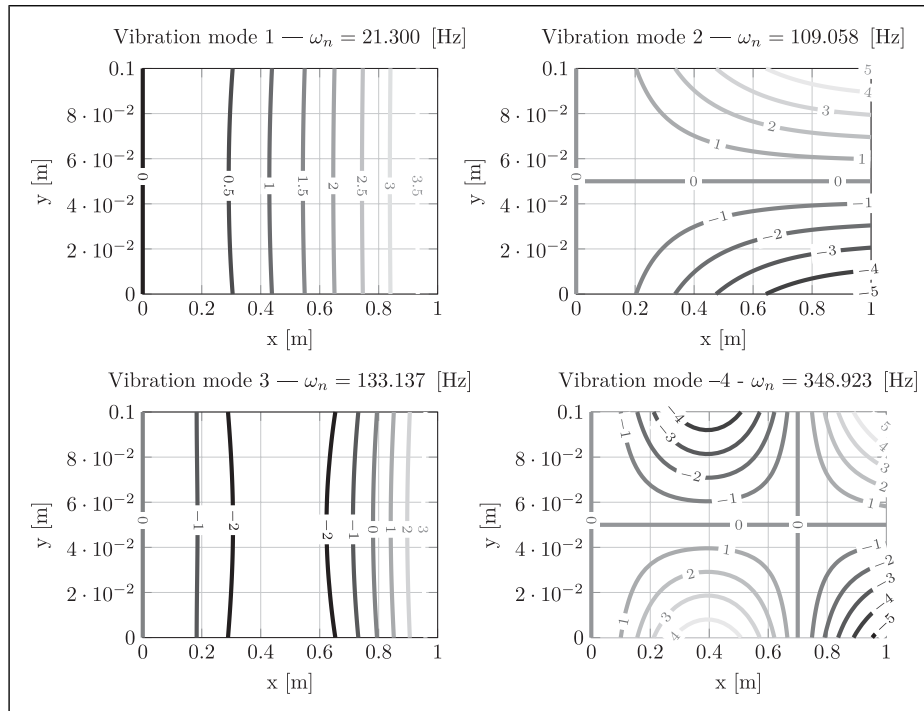


**Figure 7.** Vibration modes of the cantilever plate model.

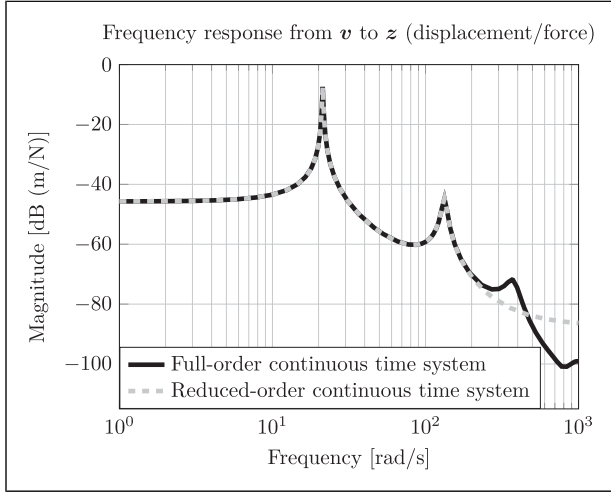


**Figure 8.** Frequency response of the reduced model to the first three vibration modes of the cantilever plate. The reduced-order model frequency response shows two peaks, corresponding to vibration modes 1 and 3. Mode 2 is a torsional one (Figure 7).

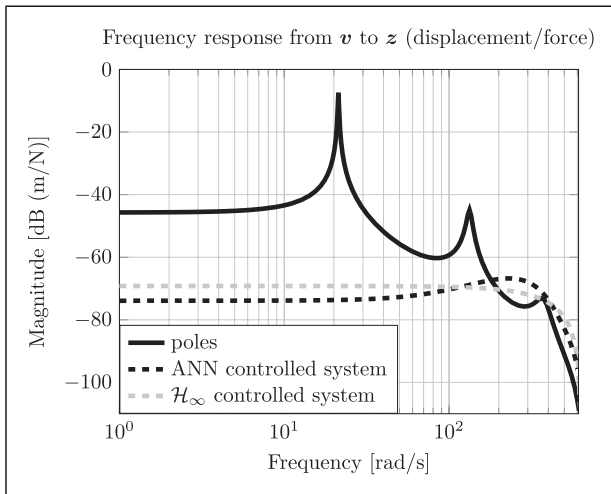


**Figure 9.** Frequency response of the cantilever plate controlled with artificial neural network and with  $\mathcal{H}_\infty$  full model.

(Rayleigh, 1877). To obtain a damping ratio lower than 5% for the three first natural frequencies, the values of  $\alpha_1 = 0.0005$  and  $\alpha_2 = 0.0500$  were selected. Table 1 shows the poles and the respective values of damping ratios and natural frequencies, with the poles of the system in the complex plane defined as  $p = -\omega_n(\zeta \pm i\sqrt{1 - \zeta^2})$ , where  $\zeta$  is the damping ratio and  $\omega_n$  is the natural frequency.

Figure 6 shows the frequency response diagram of the cantilever plate model. The vibration mode shapes from 1 to 4 are seen in Figure 7.

The obtained plant model was discretized using the method of the zero-order hold. The sampling time was chosen according to the Nyquist criterion (Nyquist, 1928). In this case, the frequency band of interest is composed of frequencies below the third peak (fifth vibration mode) in the frequency diagram (Figure 6). The third peak is present at  $\omega = 376.0$  rad/s. It presents an attenuation of the disturbance of  $-73$  dB. Therefore, the sampling frequency must be  $\omega_s \geq 752.00$  rad/s or  $F_s \geq 119.68$  Hz. So, it is possible to take safely  $F_s = 200$  Hz, which corresponds to the sampling time  $T_s = 0.005$  s.

### 3.2. Cantilever plate model reduction

The finite element model of the plate used in the preceding section has 105 nodes with three degrees of freedom per node ( $z$  axis displacement and  $x$  and  $y$  axes rotations) (Przemieniecki, 1985). Nodes 1, 22, 43, 64, and 85 are clamped. Therefore, the model has 100 free nodes, that is 300 degrees of freedom, and thus, the state-space model has 600 states. This model can be considered large in this type of control application. To have a more feasible numerical treatment for the controller design, it is convenient to have a reduced-order model.

It is important to note that the reduction of the model is performed to have a more feasible treatment in the controller design phase. However, the closed-loop system is obtained with the full-order system and the controller designed with the reduced model of the plant. This situation can be considered more realistic, leading to dynamic

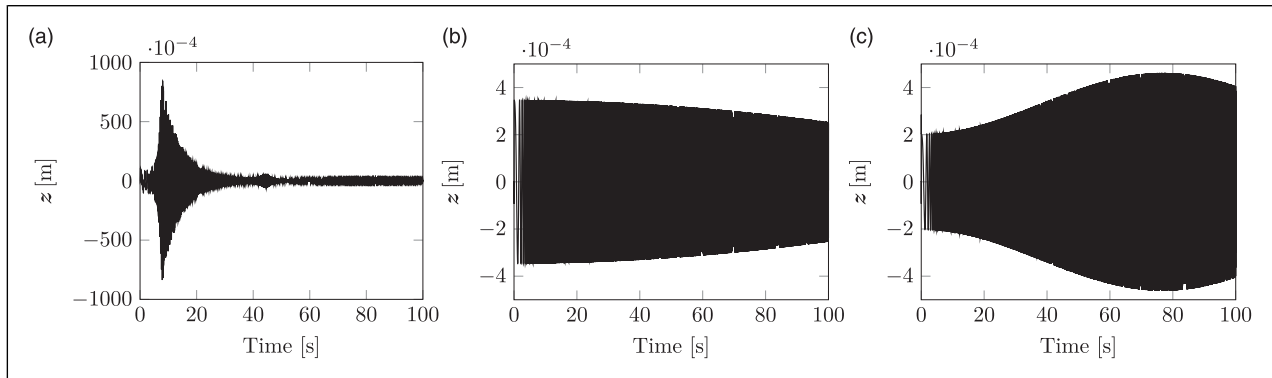


**Figure 10.** Temporal responses of the cantilever plate full model. Notice that the subfigures have different axis y scales. For the open-loop  $\pm 0.1$  m and for the closed-loop systems  $\pm 400$   $\mu\text{m}$ .

uncertainties (controller designed with a reduced model that does not have all dynamic effects of the real plant).

The most common and straightforward technique for model reduction is the model truncation, where the vibration modes higher than a critical frequency value of interest are discarded. In this case, only the first three vibration modes were held. Figure 8 shows the frequency response diagrams of the full-order model and the reduced model.

## 4. Results

The application examples were also treated using the  $\mathcal{H}_\infty$  control method. This method is a robust control technique that is widely used in the linear control theory (Fracopoulos, 1988). To benchmark the obtained results, it was considered the standard formulation of the  $\mathcal{H}_\infty$  controller. Weighting functions were not used to surpass the  $\mathcal{H}_\infty$  limitations involved in the basic and classical formulation having

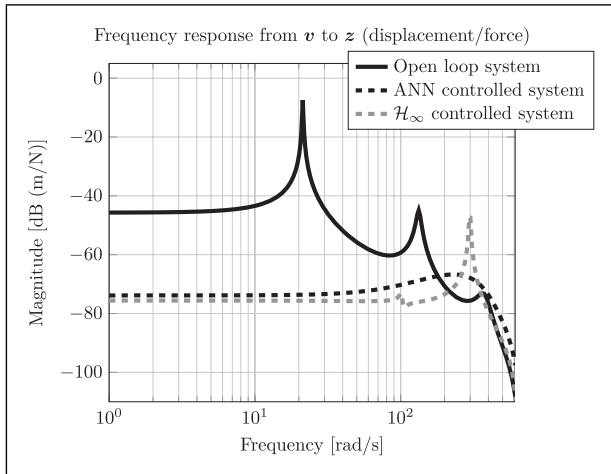


**Figure 11.** Frequency response of the cantilever plate (reduced model) controlled with artificial neural network and with  $\mathcal{H}_\infty$ .

a comparison under the same situations with the proposed technique.

For both, the ANN direct inverse and  $\mathcal{H}_\infty$  control systems, the results are presented as the time and frequency responses and the  $\mathcal{H}_\infty$  norm as a performance measurement. The temporal responses were obtained by applying as a disturbance signal a swept-sine signal of unit amplitude in the range from  $\omega_{\min} = 1$  rad/s to  $\omega_{\max} = 300$  rad/s. It is worth noting that for the performed simulations, no additive noise nor the delayed response of the control or measurement signals was taken into account.

A more detailed description of the ANN and  $\mathcal{H}_\infty$  controllers obtaining process can be found in Appendices 2 and 3, respectively. In addition, in Appendix 2, a stability analysis of the closed-loop system is made.

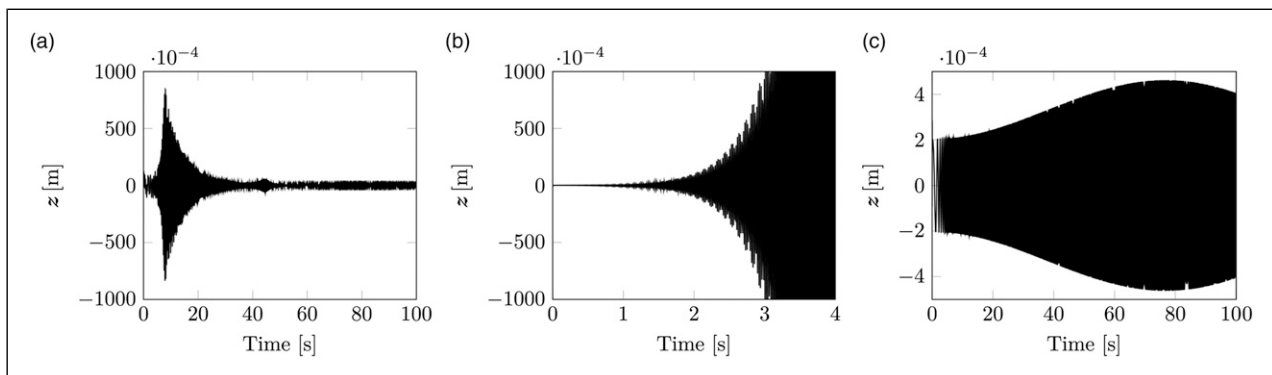
### 4.1. Cantilever plate—full model

Figure 9 shows the frequency response diagrams of the open-loop system, the controlled system with ANN, and the controlled system with the  $\mathcal{H}_\infty$  method for the full-order model. The initial attenuation of the displacement measurement obtained with ANN was 68 dB, and the initial attenuation obtained with  $\mathcal{H}_\infty$  was 72 dB.

Figure 10 shows the temporal responses of the system. The maximum plate displacements were around 0.08 m, 350  $\mu\text{m}$ , and 450  $\mu\text{m}$  for the open-loop system,  $\mathcal{H}_\infty$  controlled system, and ANN controlled system, respectively. It must be noticed that the axis  $y$  scales of Figure 10 are  $\pm 0.1$  m and  $\pm 400$   $\mu\text{m}$  for the open-loop and closed-loop systems, respectively.

### 4.2. Cantilever plate with model reduction

The frequency response of the model without control, the controlled model with ANN, and  $\mathcal{H}_\infty$  is provided in Figure 11 for the designed controller with the reduced model.



**Figure 12.** Temporal responses of the cantilever plate (reduced model). The subfigures have different axis  $y$  scales. The scale for the open-loop system and the  $\mathcal{H}_\infty$  controlled system is  $\pm 0.1$  m and for the artificial neural network controlled system is  $\pm 400$   $\mu\text{m}$ .

**Table 2.**  $\mathcal{H}_\infty$  norms comparison.

Model	$\mathcal{H}_\infty$ norm		
	Open-loop (dB)	$\mathcal{H}_\infty$ controlled (dB)	Artificial neural network controller (dB)
Full order	−7.4356	−69.1902	−66.7692
Reduced order	−7.4356	<b>Unstable</b>	−66.7377

The maximum displacement of the open-loop system was around 0.08 m, Figure 12(a), and 450  $\mu\text{m}$  for the ANN controlled system, Figure 12(c). In the case of the  $\mathcal{H}_\infty$  controlled system, the closed-loop became unstable, Figure 12(b).

The instability obtained in the  $\mathcal{H}_\infty$  closed-loop is an issue known as spillover, and it is discussed in the literature (Cabello, 2014; Gawronski, 2004; Kida and Ikeda, 1989; Sarracini, 2006). In control systems, the spillover effect refers to the control action that excites the vibration modes that were not included in the model, and in some cases, this situation can turn the closed-loop unstable.

### 4.3. $\mathcal{H}_\infty$ norms

In this section, a comparison of the results based on the  $\mathcal{H}_\infty$  norms for the examples is performed. Table 2 presents a summary of the  $\mathcal{H}_\infty$  norms for the evaluated systems.

## 5. Conclusions

As the main objective of this paper, the direct inverse control method based on the ANN was studied. This control technique was applied to the active control problem of vibrations in flexible structures. To evaluate the method, a control problem has been proposed and treated by this technique.

For the application of vibration control in a cantilever plate, the model was obtained using the FEM. In the full-order model, the plant was successfully controlled, achieving an acceptable performance compared with the solution obtained with the  $\mathcal{H}_\infty$  control method.

For the second example, a model reduction was made. In this case, the controller designed by  $\mathcal{H}_\infty$  did not achieve an adequate performance, making the temporal response unstable and leading it to saturation. On the other hand, the obtained ANN controller achieved an acceptable response mitigating the effect of disturbance in performance measurement, reducing the  $\mathcal{H}_\infty$  norm significantly, showing a good ability to deal with dynamic uncertainties generated by the reduction of the model.

From the obtained results, it was verified that the method is effective in solving certain types of control problems. The presented method is sufficiently robust in the verified examples. It has advantages compared with the  $\mathcal{H}_\infty$  method.

This method does not need a formal model of the plant because the controller is obtained based on experimental data. This situation offers vast potential in the active vibration control or areas where a mathematical model that describes the problem is not available or its deduction implies a difficult task. Another compelling advantage is that this control scheme dealt adequately with dynamic uncertainties, providing a stable temporal response by reducing the influence of the disturbance in the performance measure.

### Declaration of conflicting interests

The author(s) declared no potential conflicts of interest with respect to the research, authorship, and/or publication of this article.

### Funding

The author(s) disclosed receipt of the following financial support for the research, authorship, and/or publication of this article: This study was financed in part by the Coordenação de Aperfeiçoamento de Pessoal de Nível Superior – Brasil (CAPES) — Finance Code 001.

### ORCID iDs

William Camilo Ariza-Zambrano  <https://orcid.org/0000-0001-5151-8406>

### Notes

- 1 Notation:  $\mathbf{A}^\top$  is the transpose of  $\mathbf{A}$ .
- 2 Notation:  $\mathcal{L}^{-1}$  is the inverse Laplace transform operator.
- 3 Notation:  $i$  is the imaginary unit ( $i = \sqrt{-1}$ ).

### References

- Abreu G, Teixeira R and Ribeiro J (2000) A neural network-based direct inverse control for active control of vibrations of mechanical systems. In: Sixth Brazilian symposium on neural networks, Rio de Janeiro, Brazil, 25–25 November 2000, pp. 107–112. Los Alamitos, CA: IEEE Computer Society Press.
- Banavar RN and Dominic P (1995) An LQG/H/sub  $\infty$ /controller for a flexible manipulator. *IEEE Transactions on Control Systems Technology* 3(4): 409–416.
- Bittanti S and Piroddi L (1993) Minimum variance control of a class of nonlinear plants with neural networks. In: Third international conference on artificial neural networks, Brighton, UK, 25–27 May 1993, pp. 168–171. London: IET.

- Cabello R (2014) *Projeto de controladores  $\mathcal{H}_\infty$  de ordem reduzida e compensação de saturação em estruturas flexíveis*. PhD Thesis, University of Campinas, Brazil.
- Canahuire R and Serpa AL (2017) Reduced order  $\mathcal{H}_\infty$  controller design for vibration control using genetic algorithms. *Journal of Vibration and Control* 23(10): 1693–1707.
- Chun-Lian L and Tsai-Yuan L (2002) Neural net-based  $\mathcal{H}_\infty$  control for a class of nonlinear systems. *Neural Processing Letters* 15(2): 157–177.
- Darus I and Tokhi M (2005) Soft computing-based active vibration control of a flexible structure. *Engineering Applications of Artificial Intelligence* 18(1): 93–114.
- Fauzi B, Abderrazak C and Tarek G (2004) Internal model control using neural networks. In: Industrial technology, IEEE ICIT 04 2004 IEEE international conference, Hammamet, Tunisia, 8–10 December 2004, pp. 1121–1126. Piscataway, NJ: IEEE Press.
- Forrai A, Hashimoto S, Funato H, et al. (2000) Fuzzy logic based vibration suppression control of flexible structures. In: 6th International workshop on advanced motion control, Nagoya, Japan, 30 March–1 April 2000, pp. 378–383. Piscataway, NJ: IEEE Press.
- Fracopoulos D (1988) A course in  $\mathcal{H}_\infty$  control theory, B. A. Francis, Springer Verlag, 1987. DM 34.50, xi + 156pp. *International Journal of Adaptive Control and Signal Processing* 2(2): 151.
- Fuli W, Mingzhong L and Yinghua Y (1997) Neural network pole placement controller for nonlinear systems through linearisation. In: Proceedings of the 1997 American control conference, Albuquerque, NM, 6 June 1997, pp. 1984–1988. Piscataway, NJ: IEEE Press.
- Fuller C, Elliott S and Nelson P (1996) *Introduction to Mechanical Vibration*. San Diego, CA: Academic Press.
- Gates R, Choi M, Biswas S, et al. (1993) Stabilization of flexible structures using artificial neural networks. In: Proceedings of 1993 international conference on neural networks, Nagoya, Japan, 25–29 October 1993, pp. 1817–1820. Piscataway, NJ: IEEE Press.
- Gawronski WK (2004) *Advanced Structural Dynamics and Active Control of Structures*. Gawronski WK (ed). New York: Springer.
- Kida T and Ikeda M (1989) Robust control for large space structures: spillover suppression by frequency-shaped optimal regulator. *IFAC Proceedings Volumes* 22(7): 165–170.
- Kundu S, Seto K and Sugino S (2002) Genetic algorithm application to vibration control of tall flexible structures. In: Electronic design, test and applications, the first IEEE international workshop, Christchurch, New Zealand, 29–31 January 2002, pp. 333–337. Los Alamitos, CA: IEEE Computer Society Press.
- Lim KB, Maghami PG and Joshi SM (1992) Comparison of controller designs for an experimental flexible structure. *IEEE Control Systems* 12(3): 108–118.
- Ljung L (1999) *System Identification: Theory for the User*. 2nd edition. NJ, USA: Prentice Hall.
- Lublin L and Athans M (1994) Experimental comparison of  $\mathcal{H}_2$  and  $\mathcal{H}_\infty$  designs for a flexible structure. In: Proceedings of 1994 33rd IEEE conference on decision and control, Lake Buena Vista, FL, 14–16 December 1994, pp. 2910–2915. Piscataway, NJ: IEEE Press.
- Marquardt DW (1963) An algorithm for least-squares estimation of nonlinear parameters. *Journal of the Society for Industrial and Applied Mathematics* 11(2): 431–441.
- Moser AN (1993) Designing controllers for flexible structures with  $\mathcal{H}$ -infinity/ $\mu$ -synthesis. *IEEE Control Systems* 13(2): 79–89.
- Nørgaard M, Ravn O, Poulsen N, et al. (2004) *Neural Networks for Modelling and Control of Dynamic Systems: A Practitioner's Handbook*. London, UK: Springer-Verlag.
- Nyquist H (1928) Certain topics in telegraph transmission theory. *Transactions of the American Institute of Electrical Engineers* 47(2): 617–644.
- Ogata K (1987) *Discrete-Time Control Systems*. Upper Saddle River, NJ: Prentice-Hall.
- Przemieniecki J (1985) *Theory of Matrix Structural Analysis*. Mineola, NY: Dover Publications, Incorporated.
- Rayleigh J (1877) *The Theory of Sound*. 2nd edition. London, UK: Macmillan, Vol. 1.
- Sarracini F (2006) *Síntese de controladores  $\mathcal{H}_\infty$  de ordem reduzida com aplicação no controle ativo de estruturas flexíveis*. Master's Thesis, University of Campinas, Brazil.
- Smith RS, Cheng-Chih Chu C and Fanson JL (1994) The design of  $\mathcal{H}_\infty$  controllers for an experimental non-collocated flexible structure problem. *IEEE Transactions on Control Systems Technology* 2(2): 101–109.
- Sznaier M and Rotstein H (1992) Robust controller design for a constrained flexible structure via mixed  $l_\infty/\mathcal{H}_\infty$  optimization. In: The first IEEE conference on control applications, Dayton, OH, 13–16 September 1992, pp. 271–276. Piscataway, NJ: IEEE Press.
- Tavakolpour AR, Mailah M, Mat Darus IZ, et al. (2010) Self-learning active vibration control of a flexible plate structure with piezoelectric actuator. *Simulation Modelling Practice and Theory* 18(5): 516–532.
- Zhou K and Doyle J (1998) *Essentials of Robust Control*. Upper Saddle River, NJ: Prentice Hall.

## Appendix I. Cantilever plate in bending

In this work, the cantilever plate model is obtained by the FEM. The plant is described by the differential equation of motion of a generic mechanical structure described as

$$\mathcal{M}\ddot{\mathbf{q}}(t) + \mathcal{C}\dot{\mathbf{q}}(t) + \mathcal{K}\mathbf{q}(t) = \mathbf{B}_0\mathbf{f}(t) \quad (8)$$

or also

$$\ddot{\mathbf{q}}(t) = -\mathcal{M}^{-1}\mathcal{C}\dot{\mathbf{q}}(t) - \mathcal{M}^{-1}\mathcal{K}\mathbf{q}(t) + \mathcal{M}^{-1}\mathbf{B}_0\mathbf{f}(t) \quad (9)$$

where  $\mathbf{q}$  is the displacement,  $\mathcal{M}$  is the mass matrix,  $\mathcal{C}$  is the damping matrix,  $\mathcal{K}$  is the stiffness matrix,  $\mathbf{f}(t)$  is the external force vector, and  $\mathbf{B}_0$  is the external force location matrix. In this work, the external force vector  $\mathbf{f}(t)$  is composed of two inputs, the disturbance  $\mathbf{v}$  and the control input  $\mathbf{u}$ . Thus, the input location matrix  $\mathbf{B}_0$  is composed of the matrices  $\mathbf{B}_{0v}$  and  $\mathbf{B}_{0u}$ , the input location matrices for the disturbance and the control effort, respectively.

The state-space vector can be taken as

$$\mathbf{x}(t) = \begin{bmatrix} \mathbf{q}(t) \\ \dot{\mathbf{q}}(t) \end{bmatrix} \quad (10)$$

So, the model represented in the state-space equations is

$$\begin{aligned}\dot{\mathbf{x}}(t) &= \mathbf{A}\mathbf{x}(t) + \mathbf{B}_1\mathbf{v}(t) + \mathbf{B}_2\mathbf{u}(t) \\ \mathbf{z}(t) &= \mathbf{C}_1\mathbf{x}(t) + \mathbf{D}_{11}\mathbf{v}(t) + \mathbf{D}_{12}\mathbf{u}(t) \\ \mathbf{y}(t) &= \mathbf{C}_2\mathbf{x}(t) + \mathbf{D}_{21}\mathbf{v}(t) + \mathbf{D}_{22}\mathbf{u}(t)\end{aligned}\quad (11)$$

where matrix  $\mathbf{A}$  is defined as

$$\mathbf{A} = \begin{bmatrix} \mathbf{0} & \mathbf{I} \\ -\mathcal{M}^{-1}\mathcal{K} & -\mathcal{M}^{-1}\mathcal{C} \end{bmatrix}\quad (12)$$

and  $\mathbf{B}_1$  and  $\mathbf{B}_2$  are assembled with the structure  $[\mathbf{0} \ \mathcal{M}^{-1}\mathbf{B}_0]^\top$ , with a position matrix  $\mathbf{B}_0$  for every input  $\mathbf{v}$  and  $\mathbf{u}$ , respectively.<sup>1</sup> The matrices  $\mathbf{C}_1$ ,  $\mathbf{D}_{11}$ , and  $\mathbf{D}_{12}$  are assembled to define the performance output in terms of the state-space vector and external forces. In the same way, the matrices  $\mathbf{C}_2$ ,  $\mathbf{D}_{21}$ , and  $\mathbf{D}_{22}$ , which define the output measurements of the system, are assembled.

In this work, the proportional damping model is used (Rayleigh, 1877)

$$\mathcal{C} = \alpha_1\mathcal{K} + \alpha_2\mathcal{M}\quad (13)$$

where  $\alpha_1$  and  $\alpha_2$  are real scalars. This damping model is also known as Rayleigh damping or classical damping. As reported in Section 3.1, the values of  $\alpha_1 = 0.0005$  and  $\alpha_2 = 0.0500$  were selected to obtain a damping ratio lower than 5% for the three first natural frequencies.

For the numerical evaluation of the modeled system and its implementation in digital computers, it is necessary to discretize the continuous-time model obtained. This model can be discretized using the zero-order hold method, which assumes that the system inputs are constant during the time interval  $T_s$  (Ogata, 1987). So, the system in discrete time is described by the following difference equations

$$\begin{aligned}\mathbf{x}(k+1) &= \mathbf{A}_d\mathbf{x}(k) + \mathbf{B}_{d1}\mathbf{w}(k) + \mathbf{B}_{d2}\mathbf{u}(k) \\ \mathbf{z}(k) &= \mathbf{C}_{d1}\mathbf{x}(k) + \mathbf{D}_{d11}\mathbf{w}(k) + \mathbf{D}_{d12}\mathbf{u}(k) \\ \mathbf{y}(k) &= \mathbf{C}_{d2}\mathbf{x}(k) + \mathbf{D}_{d21}\mathbf{w}(k) + \mathbf{D}_{d22}\mathbf{u}(k)\end{aligned}\quad (14)$$

with<sup>2</sup>

$$\mathbf{A}_d = e^{\mathbf{A}T_s} = \mathcal{L}^{-1}\{(s\mathbf{I} - \mathbf{A})^{-1}\}_{t=T_s}\quad (15a)$$

$$\mathbf{B}_d = \left( \int_{\tau=0}^{T_s} e^{\mathbf{A}\tau} d\tau \right) \mathbf{B}\quad (15b)$$

$$\mathbf{C}_d = \mathbf{C}\quad (15c)$$

$$\mathbf{D}_d = \mathbf{D}\quad (15d)$$

### A. Full-order plant model

The plant model was obtained using the FEM, with the formulation of a rectangular plate in bending given in Przemieniecki (1985). The finite element mesh used is shown in Figure 5.

The FEM model plate has 100 free nodes. The rectangular element of the plate in bending proposed by

Przemieniecki (1985) has three degrees of freedom per node. Considering the state-space vector defined in equation (10), the plant order is 600.

The state-space plant model is defined according to equation (11). For this, it is necessary to define the matrices  $\mathbf{A}$ ,  $\mathbf{B}_1$ ,  $\mathbf{B}_2$ ,  $\mathbf{C}_1$ ,  $\mathbf{D}_{11}$ ,  $\mathbf{D}_{12}$ ,  $\mathbf{C}_2$ ,  $\mathbf{D}_{21}$ , and  $\mathbf{D}_{22}$ .

The input matrix  $\mathbf{B}_1$  associated with the disturbance signal  $\mathbf{v}$ , which is a punctual force in the direction of the axis  $z$ , applied on the node 50, is defined as

$$\mathbf{B}_1 = \begin{bmatrix} \mathbf{0} \\ \mathcal{M}^{-1}\mathbf{B}_{0v} \end{bmatrix} \quad \text{with} \quad \mathbf{B}_{0v} = \begin{bmatrix} \vdots \\ 0 \\ 1 \\ 0 \\ \vdots \end{bmatrix} u_{139}\quad (16)$$

and  $u_{139}$  is the degree of freedom related to the displacement in the  $z$ -axis direction of the 50th node. The input matrix  $\mathbf{B}_2$ , associated with the control signal  $\mathbf{u}$ , a force in the direction of the  $z$ -axis applied on the node 62, is given according to equation (17), and  $u_{175}$  is the degree of freedom associated with the displacement in the  $z$ -axis direction of the 62nd node

$$\mathbf{B}_2 = \begin{bmatrix} \mathbf{0} \\ \mathcal{M}^{-1}\mathbf{B}_{0u} \end{bmatrix} \quad \text{with} \quad \mathbf{B}_{0u} = \begin{bmatrix} \vdots \\ 0 \\ 1 \\ 0 \\ \vdots \end{bmatrix} u_{175}\quad (17)$$

and the output matrices  $\mathbf{C}_1$ ,  $\mathbf{D}_{11}$ , and  $\mathbf{D}_{12}$  associated with performance measurement  $\mathbf{z}$ , that is the displacement in the  $z$ -axis of node 62, are

$$\mathbf{C}_1 = \begin{bmatrix} \cdots & u_{175} & \cdots \\ \cdots & 0 & 1 & 0 & \cdots \end{bmatrix}\quad (18a)$$

$$\mathbf{D}_{11} = 0, \quad \text{and}\quad (18b)$$

$$\mathbf{D}_{12} = 0\quad (18c)$$

Also, the output matrices  $\mathbf{C}_2$ ,  $\mathbf{D}_{21}$ , and  $\mathbf{D}_{22}$  associated with the measurement signal  $\mathbf{y}$ , that is equal to the performance measurement  $\mathbf{z}$ , are defined as

$$\mathbf{C}_2 = \begin{bmatrix} \cdots & u_{175} & \cdots \\ \cdots & 0 & 1 & 0 & \cdots \end{bmatrix}\quad (19a)$$

**Table 3.** Poles of the full-order discrete state-space plant model.

Pole	Magnitude
$(9.94 \pm 1.06i) \times 10^{-1}$	$9.99 \times 10^{-1}$
$(8.42 \pm 5.11i) \times 10^{-1}$	$9.85 \times 10^{-1}$
$(7.69 \pm 6.04i) \times 10^{-1}$	$9.78 \times 10^{-1}$
$(-1.43 \pm 8.47i) \times 10^{-1}$	$8.59 \times 10^{-1}$
$(1.15 \pm 1.95i) \times 10^{-1}$	$2.27 \times 10^{-1}$

$$\mathbf{D}_{21} = 0, \quad \text{and} \quad (19b)$$

$$\mathbf{D}_{22} = 0 \quad (19c)$$

The first 10 poles of the full-order plant are seen in Table 3.<sup>3</sup>

### B. Plant model with dynamic uncertainties

To test the proposed method robustness with respect to dynamic uncertainties, and for a more feasible computational treatment, the full-order model was truncated using the first three vibration modes. To accomplish this task, the plant model is converted to the modal canonical form (function canon of MATLAB), and then, the model reduction is made (function modreal of MATLAB). The reduced model matrices are

$$\mathbf{A}_d = \begin{bmatrix} 0.993 & 0.106 & 0 & 0 & 0 & 0 \\ -0.106 & 0.993 & 0 & 0 & 0 & 0 \\ 0 & 0 & 0.842 & 0.510 & 0 & 0 \\ 0 & 0 & -0.510 & 0.842 & 0 & 0 \\ 0 & 0 & 0 & 0 & 0.769 & 0.603 \\ 0 & 0 & 0 & 0 & -0.603 & 0.769 \end{bmatrix}$$

$$\mathbf{B}_d = \begin{bmatrix} -10.95 & -56.66 \\ 5.833 \times 10^{-1} & 3.019 \\ 5.754 \times 10^{-10} & 3.786 \times 10^{-10} \\ 1.052 \times 10^{-9} & -9.226 \times 10^{-10} \\ 7.933 & -10.31 \\ 2.574 & 3.346 \end{bmatrix} \times 10^{-4}$$

$$\mathbf{C}_d = \begin{bmatrix} -0.08772 & -0.08772 \\ 5363.0 & 5363.0 \\ 4.4 \times 10^{-9} & 4.4 \times 10^{-9} \\ 1.121 \times 10^{-8} & 1.121 \times 10^{-8} \\ -2.92 & -2.92 \\ 2995.0 & 2995.0 \end{bmatrix}^T \times 10^{-4}$$

$$\mathbf{D}_d = \begin{bmatrix} 4.376 & 9.175 \\ 4.376 & 9.175 \end{bmatrix} \times 10^{-5} \quad (20)$$

The poles of the reduced-order plant are seen in Table 4.

**Table 4.** Poles of the reduced-order discrete state-space plant model.

Pole	Magnitude
$(9.94 \pm 1.06i) \times 10^{-1}$	$9.99 \times 10^{-1}$
$(8.42 \pm 5.11i) \times 10^{-1}$	$9.85 \times 10^{-1}$
$(7.69 \pm 6.04i) \times 10^{-1}$	$9.78 \times 10^{-1}$

## Appendix 2. ANN training

The ANN used as the controller was a single-layer network of five neurons with hyperbolic tangent as the activation function.

As seen in equation (7), the controller can have as input the last  $n$  values of the plant output and the past  $m$  control signal values. For all presented applications,  $n = 10$  and  $m = 10$  were chosen. Thus, the total number of inputs of the ANN controller is 20.

In favor of obtaining the optimal controller parameters, input–output signals of the plant must be acquired. For this, some simulations were made using as the excitation signal the level change at random instances as defined in Nørgaard et al. (2004) with  $\alpha = 0.9$ . The input signal has a total duration of 500 s, and it was split in half. A half was used to

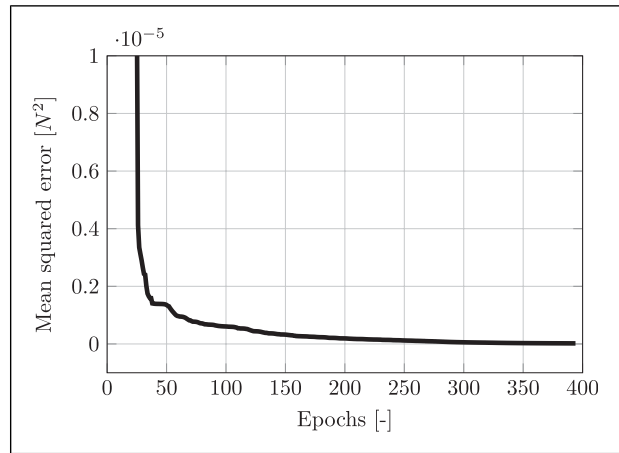


**Figure 13.** Mean squared error (Newtons squared) of the validation dataset of the controller training using the full-order plant.

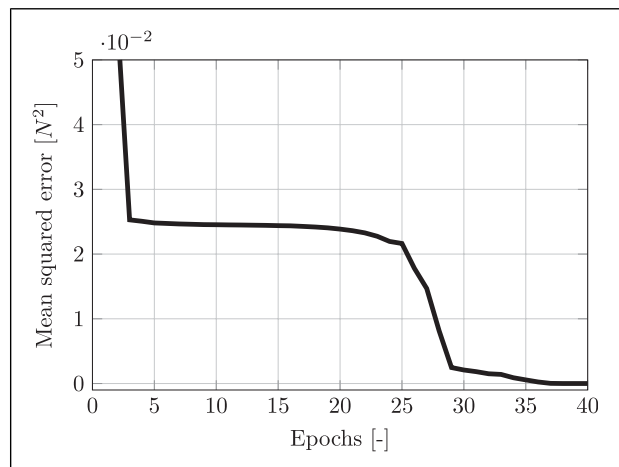


**Figure 14.** Mean squared error (Newtons squared) of the validation dataset of the controller training using the reduced-order plant.

tune the controller parameters, and the second half was used for performance validation.

As defined in equation (6), the mean squared error was used as the loss function. The optimization problem was tackled using the gradient descent-based optimization algorithm Levenberg–Marquardt (Marquardt, 1963). It was established a maximum number of epochs of 500 (the number of times that the total amount of data is presented to the optimizer). In addition, the variation of the loss function lower than  $1 \times 10^{-7}$  was used as early stopping criteria.

The values of the loss function using the validation dataset are shown in Figures 13 and 14 for the controller obtained with the full-order plant and for the reduced-order plant, respectively.

### Appendix 3. Closed-loop system stability analysis

For stability analysis, a proxy approach is proposed. In statistics, a proxy variable is the one that has a convenient correlation with an unobservable or immeasurable variable. The stability analysis is based on a proxy model of the closed-loop system. This analysis is made under the hypothesis that the identified model is a proper representation of the closed-loop system.

The proxy model is identified using the prediction error minimization approach (PEM) (Ljung, 1999). For this, the temporal impulsive response from the disturbance  $\mathbf{v}$  to the performance measurement  $\mathbf{z}$  of the closed-loop system controlled with ANN is used in this work. For the PEM application, MATLAB function `sstest` is used to obtain a state-space model in the form

$$\begin{aligned} \mathbf{x}(k+1) &= \mathbf{A}\mathbf{x}(k) + \mathbf{B}\mathbf{v}(k) \\ \mathbf{z}(k) &= \mathbf{C}\mathbf{x}(k) + \mathbf{D}\mathbf{v}(k) \end{aligned} \quad (21)$$

A linear time-invariant system is said to be stable if the transfer function has no poles on the right semiplane for the case of continuous-time models (Laplace transform domain) or no poles outside the unit circle for discrete-time models ( $\mathbf{Z}$ -transform domain).

The model order of the identified closed-loop system was selected in such a way that the associated frequency of the poles of the identified model covers a frequency range higher to the sampling frequency, that is  $F_s = 2\pi \times 200$  rad/s. To show that the identified system is an adequate representation of the closed-loop system, a fitness score was computed for every identified model. The fitness score is given by

$$\text{fit} = \frac{\|\mathbf{z} - \hat{\mathbf{z}}\|}{\|\mathbf{z} - \bar{\mathbf{z}}\|} 100\% \quad (22)$$

where  $\mathbf{z}$  is the performance measurement vector of the closed-loop system,  $\hat{\mathbf{z}}$  is the performance measurement vector of the identified closed-loop system,  $\bar{\mathbf{z}}$  is the vector

whose elements are the mean of the performance measurement vector of the closed-loop system  $\mathbf{z}$ , and  $\|\cdot\|$  refers to the computation of the Euclidean norm.

#### A. ANN controller obtained with the full-order plant

The identified model of the closed-loop system, controlled with an ANN obtained with simulations of the full-order plant, resulted in a model of order 15. The poles of the identified closed-loop system are shown in Table 5. The identified system has the poles inside the unit circle in the complex plane, which means that the closed-loop controlled with the ANN obtained with the full-order plant model is stable. The fitness score of the identified plant was 98.75%.

#### B. ANN controller obtained with the reduced-order plant

The stability analysis of the closed-loop system, controlled with an ANN obtained with the reduced-order plant model, was conducted with the same procedure previously detailed. The resulted system has order 18. The poles of the identified closed-loop model are presented in Table 6. It is possible to

**Table 5.** Poles of the closed-loop system (full-order model).

Pole	Magnitude	Frequency (rad/s)
$9.96 \times 10^{-1}$	$9.96 \times 10^{-1}$	0.81
$(8.38 \pm 4.86i) \times 10^{-1}$	$9.69 \times 10^{-1}$	105.0
$4.17 \times 10^{-1}$	$4.17 \times 10^{-1}$	175.0
$(3.38 \pm 1.47i) \times 10^{-1}$	$3.68 \times 10^{-1}$	216.0
$(1.18 \pm 1.67i) \times 10^{-1}$	$2.04 \times 10^{-1}$	371.0
$(1.30 \pm 2.55i) \times 10^{-2}$	$2.55 \times 10^{-1}$	409.0
$(-3.77 \pm 7.49i) \times 10^{-1}$	$8.39 \times 10^{-1}$	409.0
$(-9.62 \pm 7.39i) \times 10^{-3}$	$1.21 \times 10^{-2}$	1010.0
$1.39 \times 10^{-7}$	$1.39 \times 10^{-7}$	3160.0

**Table 6.** Poles of the closed-loop system (reduced-order model).

Pole	Magnitude	Frequency (rad/s)
$1.00 \times 10^{-0}$	1.00	$3.01 \times 10^{-9}$
$9.40 \times 10^{-1}$	$9.40 \times 10^{-1}$	12.5
$(8.54 \pm 4.89i) \times 10^{-1}$	$9.85 \times 10^{-1}$	104.0
$4.45 \times 10^{-1}$	$4.45 \times 10^{-1}$	162.0
$(3.17 \pm 2.04i) \times 10^{-1}$	$3.77 \times 10^{-1}$	226.0
$(4.06 \pm 8.66i) \times 10^{-1}$	$9.57 \times 10^{-1}$	227.0
$(1.75 \pm 2.89i) \times 10^{-2}$	$2.89 \times 10^{-1}$	391.0
$(-2.85 \pm 6.91i) \times 10^{-1}$	$7.48 \times 10^{-1}$	397.0
$(-4.75 \pm 5.93i) \times 10^{-1}$	$4.78 \times 10^{-1}$	621.0
$(-1.73 \pm 5.67i) \times 10^{-2}$	$5.93 \times 10^{-2}$	677.0
$5.20 \times 10^{-4}$	$5.20 \times 10^{-4}$	1510.0

**Table 7.** Poles of the  $\mathcal{H}_\infty$  controller  $\mathbf{K}$  (full-order).

Pole	Magnitude
$(8.61 \pm 4.81) \times 10^{-1}$	$9.86 \times 10^{-1}$
$(8.42 \pm 5.11) \times 10^{-1}$	$9.85 \times 10^{-1}$
$(-0.15 \pm 8.58) \times 10^{-1}$	$8.58 \times 10^{-1}$
$(-1.43 \pm 8.47) \times 10^{-1}$	$8.59 \times 10^{-1}$
$(1.06 \pm 1.97) \times 10^{-1}$	$2.24 \times 10^{-1}$

**Table 8.** Poles of the closed-loop  $\mathcal{H}_\infty$  controlled system (full-order).

Pole	Magnitude
$(8.61 \pm 4.81i) \times 10^{-1}$	$9.86 \times 10^{-1}$
$(8.42 \pm 5.11i) \times 10^{-1}$	$9.85 \times 10^{-1}$
$(8.42 \pm 5.11i) \times 10^{-1}$	$9.85 \times 10^{-1}$
$5.70 \times 10^{-1}$	$5.70 \times 10^{-1}$
$5.48 \times 10^{-1}$	$5.48 \times 10^{-1}$
$2.07 \times 10^{-1}$	$2.07 \times 10^{-1}$
$(1.48 \pm 2.73i) \times 10^{-1}$	$3.11 \times 10^{-1}$

see that there are no poles outside the unit circle, indicating that the closed-loop system using the ANN controller obtained with the reduced-order plant model is stable. The fitness score of the identified plant was 99.08%.

#### Appendix 4. $\mathcal{H}_\infty$ synthesis

To benchmark the proposed technique, the examples were also treated with the  $\mathcal{H}_\infty$  control method. The  $\mathcal{H}_\infty$  controllers aim to reduce the effects of exogenous inputs (external disturbances or measurement noise) on system performance measurements by minimizing the  $\mathcal{H}_\infty$  norm of the frequency response of the system (Zhou and Doyle, 1998). The  $\mathcal{H}_\infty$  controller  $\mathbf{K}$  is represented by the state-space form

$$\begin{aligned} \mathbf{x}_K(k+1) &= \mathbf{A}_K \mathbf{x}_K(k) + \mathbf{B}_K \mathbf{y}(k) \\ \mathbf{u}(k) &= \mathbf{C}_K \mathbf{x}_K(k) + \mathbf{D}_K \mathbf{y}(k) \end{aligned} \quad (23)$$

where  $\mathbf{x}_K(k)$  is the state vector of the controller at instant  $k$ ,  $\mathbf{A}_K$ ,  $\mathbf{B}_K$ ,  $\mathbf{C}_K$ , and  $\mathbf{D}_K$  are the state matrix, input matrix, output matrix, and feedforward matrix, respectively. The

**Table 9.** Poles of the  $\mathcal{H}_\infty$  controller  $\mathbf{K}$  (reduced-order).

Pole	Magnitude
$(8.58 \pm 4.88i) \times 10^{-1}$	$9.87 \times 10^{-1}$
$(8.42 \pm 5.11i) \times 10^{-1}$	$9.85 \times 10^{-1}$
-1.00	1.00
$-9.93 \times 10^{-1}$	$9.93 \times 10^{-1}$

**Table 10.** Poles of the closed-loop  $\mathcal{H}_\infty$  controlled system (reduced-order controller with nonreduced-order plant).

Pole	Magnitude
$6.75 \times 10^{-1}$	$6.75 \times 10^{-1}$
$(8.60 \pm 4.81i) \times 10^{-1}$	$9.86 \times 10^{-1}$
$(8.42 \pm 5.11i) \times 10^{-1}$	$9.85 \times 10^{-1}$
$(8.42 \pm 5.11i) \times 10^{-1}$	$9.85 \times 10^{-1}$
$(5.24 \pm 1.59i) \times 10^{-1}$	$5.47 \times 10^{-1}$
$(2.62 \pm 7.87i) \times 10^{-1}$	$8.30 \times 10^{-1}$

controller input is the output measurement of the plant  $\mathbf{y}$ . And the output of the controller is the control effort  $\mathbf{u}$ .

For all the presented examples, the  $\mathcal{H}_\infty$  controller synthesis was performed using the robust control toolbox of MATLAB. Specifically, the function `dhinf` was used.

#### A. Full-order plant model

A  $\mathcal{H}_\infty$  controller  $\mathbf{K}$  was computed using the full-order plant. The first 10 poles of controller  $\mathbf{K}$  are shown in Table 7.

The first 10 poles of the closed-loop system using the  $\mathcal{H}_\infty$  controller obtained with the full-order plant are shown in Table 8.

#### B. Plant model with dynamic uncertainties

A  $\mathcal{H}_\infty$  controller  $\mathbf{K}$  was computed using the reduced-order model. All the poles of controller  $\mathbf{K}$  are shown in Table 9.

It is worth noting that the obtained controller is said to be marginally stable because it has poles with unitary magnitude. The first 10 poles of the closed-loop system using the  $\mathcal{H}_\infty$  controller obtained with the reduced-order plant, but controlling the nonreduced-order plant (to check the performance considering dynamic uncertainties), are shown in Table 10.